UNIVERSAL FORMULATIONS AND COMPUTATION ALGORITHM FOR THREE-PHASE SPACE VECTOR PWM RIPPLE CURRENT ANALYSIS

Guoqiang Chen[1] and Jianli Kang[2]

[1]School of Mechanical and Power Engineering
[2]School of Computer Science and Technology
Henan Polytechnic University
No. 2001, Century Avenue, Jiaozuo 454003, P. R. China
jz97cgq@sina.com; kangjl@hpu.edu.cn

ABSTRACT. *Aiming at the complex expression and tedious derivation process, the paper discussed the analysis method to the ripple current. The universal ripple current formulations for space vector PWM (SVPWM) were given and a programming algorithm for ripple current analysis for the multi-level inverter was proposed. Finally, the ripple currents and harmonic distortion factor (HDF) expressions for a two-level inverter and a three-level one were analyzed using the algorithm, which verifies the convenience and practicability of the algorithm. It provides a powerful tool for accurately comparing the harmonic distortion performance among different PWM strategies and different level inverters, and even applicable to exploiting new PWM strategy.*
Keywords: Space vector PWM, Ripple current, Harmonic distortion factor, Inverter

1. **Introduction.** The space vector pulse width modulation (SVPWM) method, as an important subclass among all PWM techniques, has been widely used to convert electric energy between direct current source and alternating current source [1]. Because of the volt-second balance principle of PWM technique, the harmonic is inevitable besides the required fundamental wave [2]. The voltage source inverter has been widely used due to the simple structure and load carrying feature. The output of the voltage source inverter includes a series of pulses in the aspect of voltage [3], while the current has another shape determined by the load. The motor load presents prominent inductance [4]. The current harmonic takes the form of amplitude frequency and phase frequency characteristics in the frequency domain, while takes the form of ripple current in the time domain. The ripple current has heavy effects on the losses of the load motor [5], the dynamic operational characteristics of the closed-loop system [6], EMI (Electromagnetic Interference) [7] and audible noise [8], but it is very difficult to get the exact mathematical description for the effects [9]. The randomization [10], optimization [11], and variable modulation mode [12] methods have been developed and widely utilized. The ripple expressions differ from each other in a great number of SVPWM strategies. Holmes and Lipo [2] presented the corresponding expressions of the ripple currents and harmonics for the commonly used SVPWM strategies. Chen et al. analyzed the current harmonics of a random pulse position SVPWM [13], a random zero-vector distribution SVPWM [14] and a hybrid SVPWM based on random zero-vector distribution and random pulse position [15]. Although the ripple current formulations are derived from simple physical theories and mathematical equations, the ripple current expressions are complicated piecewise

functions [16]. The derivation process is tedious and quite error-prone. The ripple current expression forms the backbone for further research on PWM strategies.

Although the harmonic characteristic of SVPWM has gained intensive study and some significant conclusions have been drawn, several problems should be noticed. First of all, the harmonic formulation must be applied to the specific PWM strategy and lack universality. Furthermore, the formulation, depending on the specific PWM strategy, is extremely complicated. In addition, the explicit analytical expression of the harmonic current is not necessary because it is only the intermediate link for the harmonic analysis about the harmonic distortion factor, the harmonic spectrum, and so on. Last but not least, the study is aimed at the PWM strategies that are already known, but a large number of new strategies will be exploited in the future. A formulation or algorithm that is applicable for all kinds of SVPWM strategies is clearly of great benefit. Therefore, the paper gives the universal ripple current formulations for the space vector SVPWM strategy, and proposes a programming algorithm for ripple current analysis for the multi-level inverter using SVPWM technique. The algorithm makes full use of the symbolic computation function in some mathematical analysis software packages, for example, MATLAB.

This paper is organized as follows. In Section 2, the principles of SVPWM are presented for the three-phase inverter, especially the two-level inverter and the three-level inverter. Section 3 describes the derivation process of the universal ripple current formulations in detail. In Section 4, a programming algorithm is proposed for ripple current analysis based on the universal formulation derived in Section 3. In Section 5, the ripple current and harmonic distortion factor (HDF) for a two-level inverter and a three-level one are analyzed using the algorithm. Section 6 concludes this paper.

2. **Principles of SVPWM.** The classic two-level three-phase inverter topology with the DC bus voltage U_{DC} is shown in Figure 1(a) [2,3]. The inverter has 8 permissible states. If the load is an isolated neutral machine, the corresponding phase-to-neutral voltages for each state can be computed. For example, if T_2, T_4 and T_5 are turned off, using the simple circuit shown in Figure 1(b) with the impedances Z_{A}, Z_{B} and Z_{C} for phases A, B and C, the three phase-to-neutral voltages U_{A}, U_{B} and U_{C} are

$$\begin{cases} U_{\mathrm{A}} = U_{\mathrm{DC}}/3 \\ U_{\mathrm{B}} = U_{\mathrm{DC}}/3 \\ U_{\mathrm{C}} = 2U_{\mathrm{DC}}/3 \end{cases} \tag{1}$$

where U_{DC} is the DC bus voltage.

The voltage vector is constructed by

$$\vec{U} = \frac{2}{3}\left(U_{\mathrm{A}} + \alpha U_{\mathrm{B}} + \alpha^2 U_{\mathrm{C}}\right) \tag{2}$$

where $\alpha = \mathrm{e}^{\mathrm{j}2\pi/3}$ and $\alpha^2 = \mathrm{e}^{\mathrm{j}4\pi/3}$.

The operation mode of a two-level inverter gives five levels (0, $\pm U_{\mathrm{DC}}/3$ and $\pm 2U_{\mathrm{DC}}/3$) with respect to the isolated neutral. Based on Equation (2), the corresponding space vectors for the 8 states can be derived. The construction method of $\vec{U}_2(110)$ is shown in Figure 1(c). The six active vectors are

$$\vec{U}_k = \frac{2}{3}\left(U_{\mathrm{A}} + \alpha U_{\mathrm{B}} + \alpha^2 U_{\mathrm{C}}\right) = \frac{2}{3}U_{\mathrm{DC}}\mathrm{e}^{\mathrm{j}(k-1)\frac{\pi}{3}} \quad (k = 1, 2, \ldots, 6) \tag{3}$$

All the six active vectors $\left(\vec{U}_1(100), \vec{U}_2(110), \vec{U}_3(010), \vec{U}_4(011), \vec{U}_5(001) \text{ and } \vec{U}_6(101)\right)$ and the two zero vectors $\left(\vec{U}_0(000) \text{ and } \vec{U}_7(111)\right)$ are plotted in Figure 1(d). For the

(a) Two-level three-phase inverter

(b) Connection state of (110)

(c) Construction method of space vector
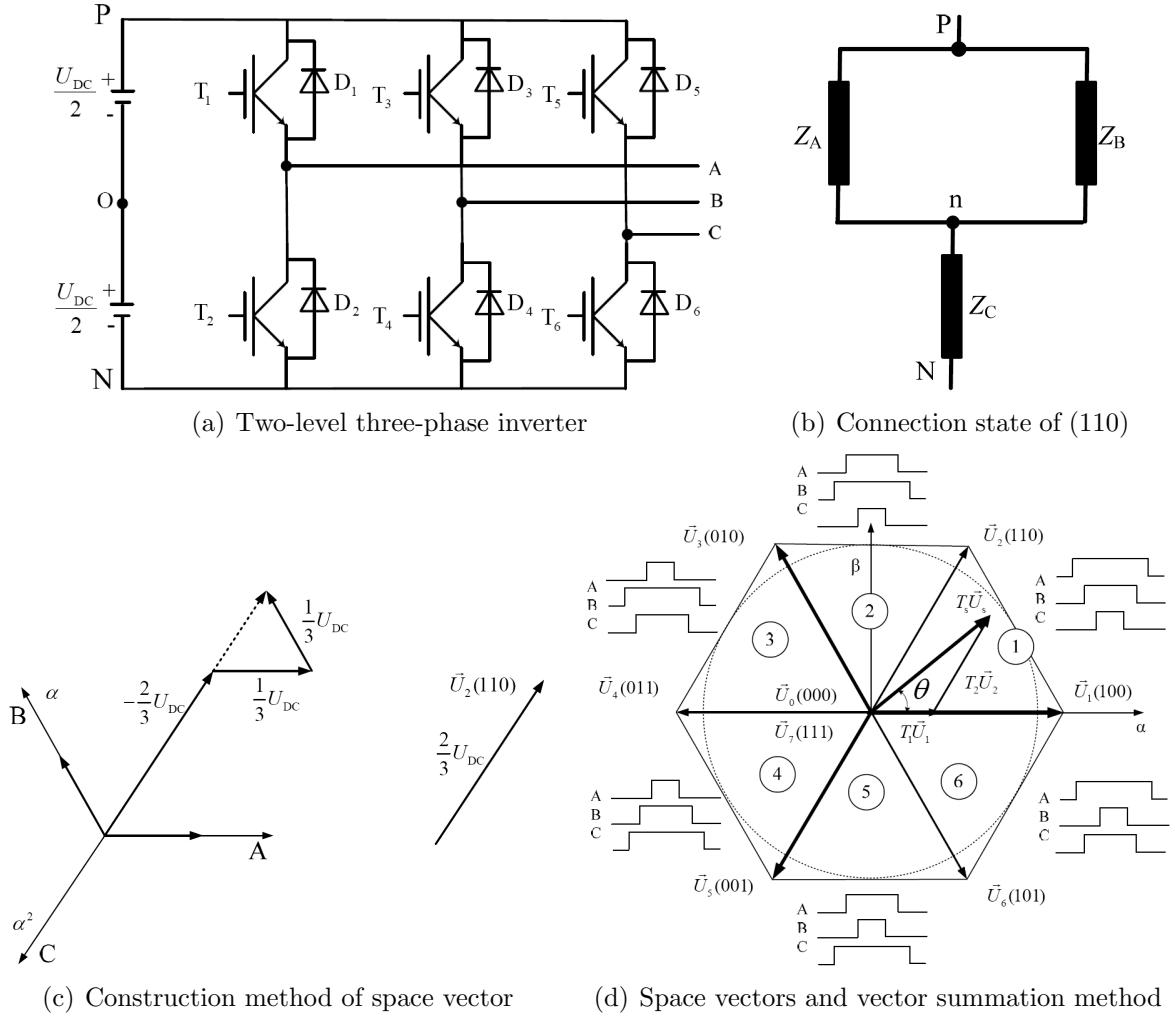
(d) Space vectors and vector summation method

FIGURE 1. Two-level inverter and vector diagram

square-wave operation of the inverter, the vector sequence is

$$\vec{U}_1(100) \to \vec{U}_2(110) \to \vec{U}_3(010) \to \vec{U}_4(011) \to \vec{U}_5(001) \to \vec{U}_6(101) \to \vec{U}_1(100) \to \cdots \quad (4)$$

The phase voltage waves have the characteristics of six-stepped wave shape, and can be expressed by Fourier series. For example, phase A

$$U_A = \frac{2U_{DC}}{\pi} \left(\cos \omega t - \frac{1}{5} \cos 5\omega t + \frac{1}{7} \cos 7\omega t - \frac{1}{11} \cos 11\omega t + \frac{1}{13} \cos 13\omega t + \cdots \right) \quad (5)$$

An arbitrary command/reference voltage vector inside the hexagon region shown in Figure 1(c) can be expressed as

$$\vec{U}_S = U_o e^{j\theta} \quad (6)$$

where U_o is the vector amplitude and θ is the phase angle.

A modulation index is given by

$$M = \frac{U_o}{U_{max}} \quad (7)$$

where U_{max} is a norm that may be the fundamental peak value $(2U_{DC}/\pi)$ of the six-stepped operation mode or half of the DC voltage value $(U_{DC}/2)$.

In the linear or undermodulation region, the constructed vector always remains within the hexagon. The maximum value of M_{max} at the end of the undermodulation region can

be derived as

$$M_{\max} = \frac{2U_{\mathrm{DC}}/3 \times \cos\frac{\pi}{6}}{U_{\max}} = \begin{cases} \dfrac{U_{\mathrm{DC}}/\sqrt{3}}{2U_{\mathrm{DC}}/\pi} = \dfrac{\pi}{2\sqrt{3}} \approx 0.9069 & \dfrac{2U_{\mathrm{DC}}}{\pi} \text{ adopted} \\[2ex] \dfrac{U_{\mathrm{DC}}/\sqrt{3}}{U_{\mathrm{DC}}/2} = \dfrac{2}{\sqrt{3}} \approx 1.1547 & \dfrac{U_{\mathrm{DC}}}{2} \text{ adopted} \end{cases} \tag{8}$$

The command voltage vector $\vec{U}_{\mathrm{S}}$ can be generated by two adjacent active vectors $\left(\vec{U}_1\right.$ and $\vec{U}_2$ in the first sextant$\left.\right)$ and the zero vectors. The on-state durations T_1, T_2 and T_0 of the three vectors are determined by identical volt-seconds balance at the periodical time interval T_{S}. The method to determine and obtain T_1, T_2 and T_0 will be found in Section 4.

$$T_{\mathrm{S}}\vec{U}_{\mathrm{S}} = T_1\vec{U}_1 + T_2\vec{U}_2 \tag{9}$$

Because of the volt-second balance of PWM, the harmonic is inevitable besides the required fundamental voltage, and so do the ripple currents. There are large numbers of vector operation modes that satisfy Equation (9).
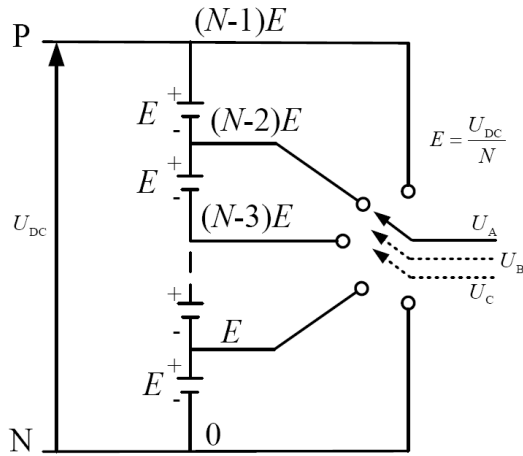
The principle of a multi-level three-phase inverter is shown in Figure 2(a) [4,17-20]. An N-level inverter gives N voltage levels $(0, U_{\mathrm{DC}}/(N-1), 2U_{\mathrm{DC}}/(N-1), \ldots, (N-2)U_{\mathrm{DC}}/(N-1), U_{\mathrm{DC}})$ with respect to the negative rail N. For example, a three-level neutral-point clamped (NPC) inverter shown in Figure 2(b) gives three voltage levels $(0, U_{\mathrm{DC}}/2$ and $U_{\mathrm{DC}})$ with respect to the negative rail N or $(-U_{\mathrm{DC}}/2, 0$ and $U_{\mathrm{DC}}/2)$ with respect to the neutral point 0 created by two identical DC link capacitors C_1 and C_2. The corresponding space vectors for the 27 states can be derived based on Equation (2). The command voltage vector $\vec{U}_{\mathrm{S}}$ can be generated by three vectors corresponding to the apexes of the triangle that includes $\vec{U}_{\mathrm{S}}$. For example, the three vectors are PPP/OOO/NNN, POO/ONN and PPO/OON, as shown in Figure 2(c). The corresponding symmetrical pattern shown in Figure 3 gives excellent harmonic characteristic. The duration time t_1, t_2, t_3 and t_4 depend on the specific SVPWM strategy and will be given in Section 4. The vector sequences in each triangle in 60°-Sextant 1 and 2 are shown in Table 1.

TABLE 1. Switching states or vector sequences beginning with positive small vector

Triangles in 60°-Sextant 1						Triangles in 60°-Sextant 2					
1(A)	2(A)	3(B)	4(B)	5(D)	6(C)	1	2	3	4	5	6
PPO	POO	PPO	POO	PPO	POO	OPO	PPO	OPO	PPO	OPO	PPO
POO	OOO	POO	PON	PPN	PON	OOO	OPO	OPN	OPO	OPN	PPN
OOO	OON	PON	OON	PON	PNN	OON	OOO	OON	OPN	NPN	OPN
OON	ONN	OON	ONN	OON	ONN	NON	OON	NON	OON	NON	OON
OOO	OON	PON	OON	PON	PNN	OON	OOO	OON	OPN	NPN	OPN
POO	OOO	POO	PON	PPN	PON	OOO	OPO	OPN	OPO	OPN	PPN
PPO	POO	PPO	POO	PPO	POO	OPO	PPO	OPO	PPO	OPO	PPO

3. **Ripple Current Formulations.** Implicit phase voltage modulation waves U_{A}, U_{B} and U_{C} and line voltages U_{AB}, U_{AC} and U_{BC} can be computed using average method in the switching period. For a two-level or three-level inverter, let
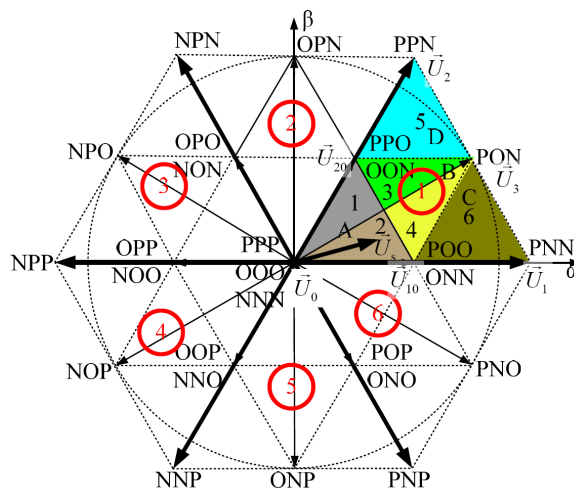
$$\begin{cases} u_{\mathrm{A}} = U_{\mathrm{A}}/(U_{\mathrm{DC}}/2) \\ u_{\mathrm{B}} = U_{\mathrm{B}}/(U_{\mathrm{DC}}/2) \\ u_{\mathrm{C}} = U_{C}/(U_{\mathrm{DC}}/2) \end{cases} \tag{10}$$

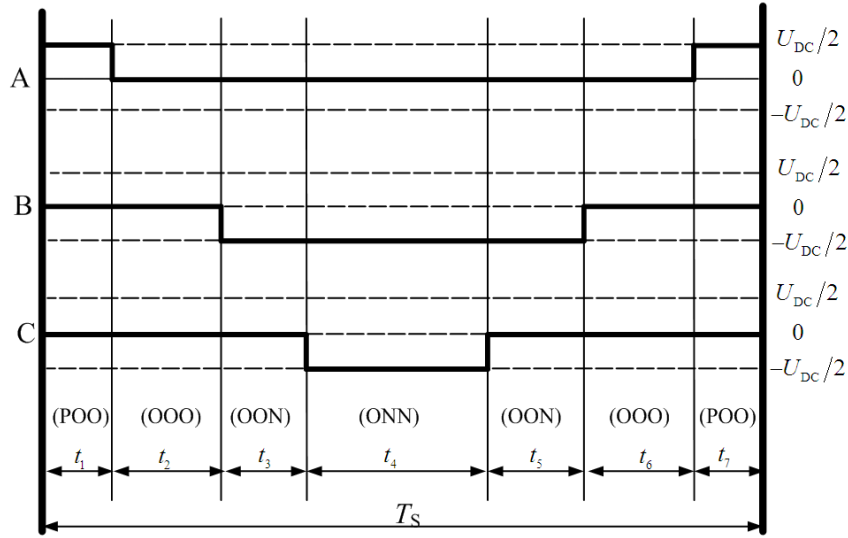(a) Multi-level three-phase inverter principle
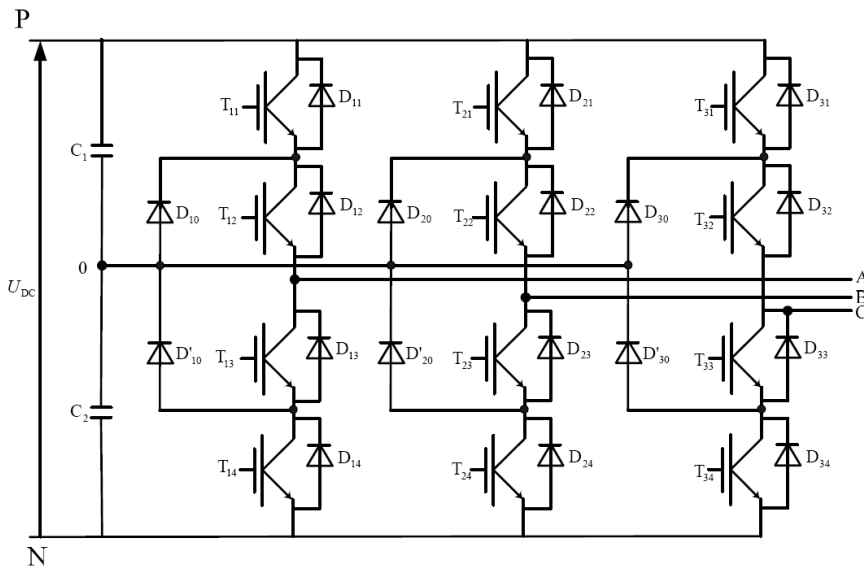
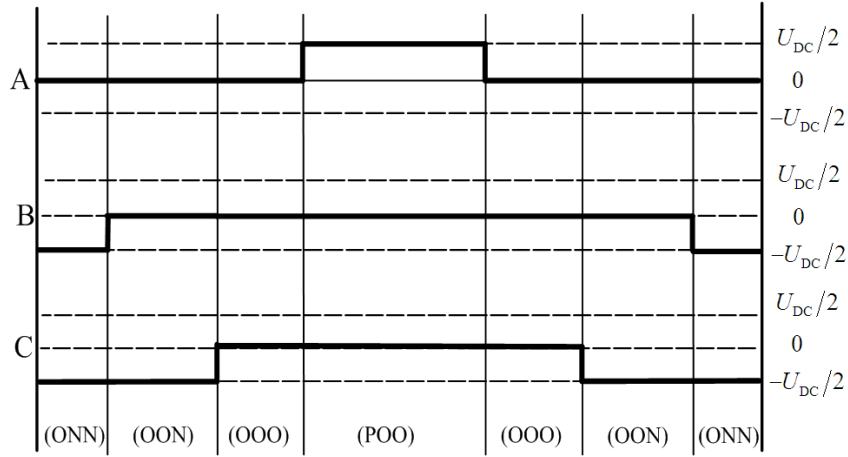(b) Three-level three-phase inverter

(c) Space vectors and vector summation method

FIGURE 2. Three-level inverter and vector diagram. The notations P, O and N refer to that the phase output terminals are positive, negative and zero, respectively.

(a) Beginning with the positive small vector

(b) Beginning with the negative small vector

FIGURE 3. PWM voltage waves for the command voltage vector $\vec{U}_S$

For the delta connection and prominent inductance load with the equivalent line-line inductance L_σ in triangle 2(A), the ripple current of line AB with respect to the time t can be expressed as

(1) $0 \leq t \leq t_1$,

$$\Delta i_{AB} = \frac{\frac{U_{DC}}{2} - U_{AB}}{L_\sigma} t = \frac{\frac{U_{DC}}{2} - \frac{U_{DC}}{2}(u_A - u_B)}{L_\sigma} t = \frac{U_{DC}}{2L_\sigma} \left[1 - (u_A - u_B) \right] t \qquad (11)$$

(2) $t_1 \leq t \leq t_1 + t_2$,

$$\begin{aligned} \Delta i_{AB} &= \frac{U_{DC}}{2L_\sigma} \left[1 - (u_A - u_B) \right] t_1 + \frac{-U_{AB}}{L_\sigma} (t - t_1) \\ &= \frac{U_{DC}}{2L_\sigma} \left\{ \left[1 - (u_A - u_B) \right] t_1 - (u_A - u_B)(t - t_1) \right\} \end{aligned} \qquad (12)$$

(3) $t_1 + t_2 \leq t \leq t_1 + t_2 + t_3$,

$$\Delta i_{AB} = \frac{U_{DC}}{2L_\sigma} \left\{ \left[1 - (u_A - u_B) \right] t_1 - (u_A - u_B)(t - t_1) \right\} \qquad (13)$$

(4) $t_1 + t_2 + t_3 \le t \le t_1 + t_2 + t_3 + t_4,$

$$
\begin{aligned}
\Delta i_{\mathrm{AB}} &= \frac{U_{\mathrm{DC}}}{2L_\sigma} \left\{ [1 - (u_{\mathrm{A}} - u_{\mathrm{B}})]\, t_1 - (u_{\mathrm{A}} - u_{\mathrm{B}})\, (t_2 + t_3) \right\} \\
&\quad + \frac{\frac{U_{\mathrm{DC}}}{2} - U_{\mathrm{AB}}}{L_\sigma} \left(t - t_1 - t_2 - t_3 \right) \\
&= \frac{U_{\mathrm{DC}}}{2L_\sigma} \left\{ [1 - (u_{\mathrm{A}} - u_{\mathrm{B}})]\, t_1 - (u_{\mathrm{A}} - u_{\mathrm{B}})\, (t_2 + t_3) \right. \\
&\quad \left. + [1 - (u_{\mathrm{A}} - u_{\mathrm{B}})]\, (t - t_1 - t_2 - t_3) \right\}
\end{aligned}
\tag{14}
$$

For the delta connection load in triangle 2(A), the ripple current of line AC can be expressed as

(1) $0 \le t \le t_1,$

$$
\Delta i_{\mathrm{AC}} = \frac{\frac{U_{\mathrm{DC}}}{2} - U_{\mathrm{AC}}}{L_\sigma} t = \frac{\frac{U_{\mathrm{DC}}}{2} - \frac{U_{\mathrm{DC}}}{2}(u_{\mathrm{A}} - u_{\mathrm{C}})}{L_\sigma} t = \frac{U_{\mathrm{DC}}}{2L_\sigma} [1 - (u_{\mathrm{A}} - u_{\mathrm{C}})]\, t
\tag{15}
$$

(2) $t_1 \le t \le t_1 + t_2,$

$$
\begin{aligned}
\Delta i_{\mathrm{AC}} &= \frac{U_{\mathrm{DC}}}{2L_\sigma} [1 - (u_{\mathrm{A}} - u_{\mathrm{C}})]\, t_1 + \frac{-U_{\mathrm{AC}}}{L_\sigma} (t - t_1) \\
&= \frac{U_{\mathrm{DC}}}{2L_\sigma} \left\{ [1 - (u_{\mathrm{A}} - u_{\mathrm{C}})]\, t_1 - (u_{\mathrm{A}} - u_{\mathrm{C}})\, (t - t_1) \right\}
\end{aligned}
\tag{16}
$$

(3) $t_1 + t_2 \le t \le t_1 + t_2 + t_3,$

$$
\begin{aligned}
\Delta i_{\mathrm{AC}} &= \frac{U_{\mathrm{DC}}}{2L_\sigma} \left\{ [1 - (u_{\mathrm{A}} - u_{\mathrm{C}})]\, t_1 - (u_{\mathrm{A}} - u_{\mathrm{C}})\, t_2 \right\} + \frac{\frac{U_{\mathrm{DC}}}{2} - U_{\mathrm{AC}}}{L_\sigma} (t - t_1 - t_2) \\
&= \frac{U_{\mathrm{DC}}}{2L_\sigma} \left\{ [1 - (u_{\mathrm{A}} - u_{\mathrm{C}})]\, t_1 - (u_{\mathrm{A}} - u_{\mathrm{C}})\, t_2 + \{1 - (u_{\mathrm{A}} - u_{\mathrm{C}})\}\, (t - t_1 - t_2) \right\}
\end{aligned}
\tag{17}
$$

(4) $t_1 + t_2 + t_3 \le t \le t_1 + t_2 + t_3 + t_4,$

$$
\Delta i_{\mathrm{AC}} = \frac{U_{\mathrm{DC}}}{2L_\sigma} \left\{ [1 - (u_{\mathrm{A}} - u_{\mathrm{C}})]\, t_1 - (u_{\mathrm{A}} - u_{\mathrm{C}})\, t_2 + \{1 - (u_{\mathrm{A}} - u_{\mathrm{C}})\}\, (t - t_1 - t_2) \right\}
\tag{18}
$$

For the delta connection load in triangle 2(A), the ripple current of line BC can be expressed as

(1) $0 \le t \le t_1,$

$$
\Delta i_{\mathrm{BC}} = \frac{-U_{\mathrm{BC}}}{L_\sigma} t = \frac{-\frac{U_{\mathrm{DC}}}{2}(u_{\mathrm{B}} - u_{\mathrm{C}})}{L_\sigma} t = -\frac{U_{\mathrm{DC}}}{2L_\sigma} (u_{\mathrm{B}} - u_{\mathrm{C}})\, t
\tag{19}
$$

(2) $t_1 \le t \le t_1 + t_2,$

$$
\Delta i_{\mathrm{BC}} = -\frac{U_{\mathrm{DC}}}{2L_\sigma} (u_{\mathrm{B}} - u_{\mathrm{C}})\, t
\tag{20}
$$

(3) $t_1 + t_2 \le t \le t_1 + t_2 + t_3,$

$$
\begin{aligned}
\Delta i_{\mathrm{BC}} &= -\frac{U_{\mathrm{DC}}}{2L_\sigma} (u_{\mathrm{B}} - u_{\mathrm{C}})\, (t_1 + t_2) + \frac{\frac{U_{\mathrm{DC}}}{2} - U_{\mathrm{BC}}}{L_\sigma} (t - t_1 - t_2) \\
&= -\frac{U_{\mathrm{DC}}}{2L_\sigma} \left\{ (u_{\mathrm{B}} - u_{\mathrm{C}})\, (t_1 + t_2) - [1 - (u_{\mathrm{B}} - u_{\mathrm{C}})]\, (t - t_1 - t_2) \right\}
\end{aligned}
\tag{21}
$$

(4) $t_1 + t_2 + t_3 \leq t \leq t_1 + t_2 + t_3 + t_4$,

$$\Delta i_{\text{BC}}$$
$$= -\frac{U_{\text{DC}}}{2L_\sigma} \left\{ (u_\text{B} - u_\text{C})(t_1 + t_2) - [1 - (u_\text{B} - u_\text{C})] t_3 \right\} + \frac{-U_{\text{BC}}}{L_\sigma} (t - t_1 - t_2 - t_3) \tag{22}$$
$$= \frac{U_{\text{DC}}}{2L_\sigma} \left\{ -(u_\text{B} - u_\text{C})(t_1 + t_2) + [1 - (u_\text{B} - u_\text{C})] t_3 - (u_\text{B} - u_\text{C})(t - t_1 - t_2 - t_3) \right\}$$

Let (S_{1i}, S_{2i}, S_{3i}) stand for the switching state of the ith working vector, and S_{ji} ($j = 1, 2, 3$) is -1, 0 and 1 for N, O and P, respectively. As discussed above, the ripple currents Equations (11) to (22) can be summarized and expressed using the following universal formulas. For example, Equation (11) is corresponding to the specific case of the first formula in Equation (23) for that $S_{11} = 1$ and $S_{21} = 0$.

(1) $0 \leq t \leq t_1$,

$$\begin{cases} \Delta i_{\text{AB}} = \dfrac{\left(S_{11} \cdot \frac{U_{\text{DC}}}{2} - S_{21} \cdot \frac{U_{\text{DC}}}{2} \right) - U_{\text{AB}}}{L_\sigma} t = \dfrac{U_{\text{DC}}}{2L_\sigma} [(S_{11} - S_{21}) - (u_\text{A} - u_\text{B})] t \\[3mm] \Delta i_{\text{AC}} = \dfrac{\left(S_{11} \cdot \frac{U_{\text{DC}}}{2} - S_{31} \cdot \frac{U_{\text{DC}}}{2} \right) - U_{\text{AC}}}{L_\sigma} t = \dfrac{U_{\text{DC}}}{2L_\sigma} [(S_{11} - S_{31}) - (u_\text{A} - u_\text{C})] t \\[3mm] \Delta i_{\text{BC}} = \dfrac{\left(S_{21} \cdot \frac{U_{\text{DC}}}{2} - S_{31} \cdot \frac{U_{\text{DC}}}{2} \right) - U_{\text{BC}}}{L_\sigma} t = \dfrac{U_{\text{DC}}}{2L_\sigma} [(S_{21} - S_{31}) - (u_\text{B} - u_\text{C})] t \end{cases} \tag{23}$$

(2) $t_1 \leq t \leq t_1 + t_2$,

$$\begin{cases} \Delta i_{\text{AB}} = \dfrac{U_{\text{DC}}}{2L_\sigma} \left\{ [(S_{11} - S_{21}) - u_{\text{AB}}] t_1 + [(S_{12} - S_{22}) - u_{\text{AB}}] (t - t_1) \right\} \\[3mm] \Delta i_{\text{AC}} = \dfrac{U_{\text{DC}}}{2L_\sigma} \left\{ [(S_{11} - S_{31}) - u_{\text{AC}}] t_1 + [(S_{12} - S_{32}) - u_{\text{AC}}] (t - t_1) \right\} \\[3mm] \Delta i_{\text{BC}} = \dfrac{U_{\text{DC}}}{2L_\sigma} \left\{ [(S_{21} - S_{31}) - u_{\text{BC}}] t_1 + [(S_{22} - S_{32}) - u_{\text{BC}}] (t - t_1) \right\} \end{cases} \tag{24}$$

(3) $t_1 + t_2 \leq t \leq t_1 + t_2 + t_3$,

$$\begin{cases} \Delta i_{\text{AB}} = \dfrac{U_{\text{DC}}}{2L_\sigma} \big\{ [(S_{11} - S_{21}) - u_{\text{AB}}] t_1 + [(S_{12} - S_{22}) - u_{\text{AB}}] t_2 \\ \qquad\qquad + [(S_{13} - S_{23}) - u_{\text{AB}}] (t - t_1 - t_2) \big\} \\[3mm] \Delta i_{\text{AC}} = \dfrac{U_{\text{DC}}}{2L_\sigma} \big\{ [(S_{11} - S_{31}) - u_{\text{AC}}] t_1 + [(S_{12} - S_{32}) - u_{\text{AC}}] t_2 \\ \qquad\qquad + [(S_{13} - S_{33}) - u_{\text{AC}}] (t - t_1 - t_2) \big\} \\[3mm] \Delta i_{\text{BC}} = \dfrac{U_{\text{DC}}}{2L_\sigma} \big\{ [(S_{21} - S_{31}) - u_{\text{BC}}] t_1 + [(S_{22} - S_{32}) - u_{\text{BC}}] t_2 \\ \qquad\qquad + [(S_{23} - S_{33}) - u_{\text{BC}}] (t - t_1 - t_2) \big\} \end{cases} \tag{25}$$

(4) $t_1 + t_2 + t_3 \leq t \leq t_1 + t_2 + t_3 + t_4$,

$$\begin{cases} \Delta i_{\text{AB}} = \dfrac{U_{\text{DC}}}{2L_\sigma} \left\{ \begin{array}{l} [(S_{11} - S_{21}) - u_{\text{AB}}] t_1 + [(S_{12} - S_{22}) - u_{\text{AB}}] t_2 \\ + [(S_{13} - S_{23}) - u_{\text{AB}}] t_3 + [(S_{14} - S_{24}) - u_{\text{AB}}] (t - t_1 - t_2 - t_3) \end{array} \right\} \\[4mm] \Delta i_{\text{AC}} = \dfrac{U_{\text{DC}}}{2L_\sigma} \left\{ \begin{array}{l} [(S_{11} - S_{31}) - u_{\text{AC}}] t_1 + [(S_{12} - S_{32}) - u_{\text{AC}}] t_2 \\ + [(S_{13} - S_{33}) - u_{\text{AC}}] t_3 + [(S_{14} - S_{34}) - u_{\text{AC}}] (t - t_1 - t_2 - t_3) \end{array} \right\} \\[4mm] \Delta i_{\text{BC}} = \dfrac{U_{\text{DC}}}{2L_\sigma} \left\{ \begin{array}{l} [(S_{21} - S_{31}) - u_{\text{BC}}] t_1 + [(S_{22} - S_{32}) - u_{\text{BC}}] t_2 \\ + [(S_{23} - S_{33}) - u_{\text{BC}}] t_3 + [(S_{24} - S_{34}) - u_{\text{BC}}] (t - t_1 - t_2 - t_3) \end{array} \right\} \end{cases} \tag{26}$$

4. **Programming Algorithm.** The symbolic computation function in the technical computing language should be used to analyze the ripple current characteristics because the symbolic computation can provide the analytical expression. Based on the ripple current Equations (23) to (26), the algorithm can be expressed as follows.

Step 1: Create symbolic variables. The variables include the switching period T_S, modulation index M, DC bus voltage U_DC, equivalent inductance L_σ and so on.

Step 2: Store the switching states and vector sequences in a matrix S for each triangle. Each column is corresponding to a voltage space vector. The format of S is shown in Figure 4.

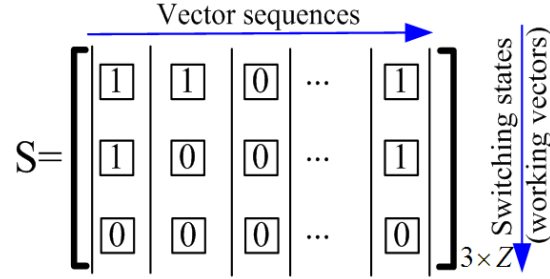
FIGURE 4. Format of switching states and vector sequences matrix S

Step 3: Compute on-state durations of the basic vectors. The on-state durations are computed based on volt-second balance. For example, the solution of (9) for the two-level inverter in the first sextant is

$$
\begin{cases}
T_1 = \dfrac{\sqrt{3}}{2} M T_\text{S} \sin\left(\pi/3 - \theta\right) \\[2mm]
T_2 = \dfrac{\sqrt{3}}{2} M T_\text{S} \sin\theta
\end{cases}
\tag{27}
$$

$$
T_1 + T_2 = \frac{\sqrt{3}}{2} M T_\text{S} \sin\left(\pi/3 + \theta\right)
\tag{28}
$$

The total duration of two zero vectors (T_{00} for $\vec{U}_0$ and T_{07} for $\vec{U}_7$) is

$$
T_0 = T_\text{S} - T_1 - T_2 = T_{00} + T_{07}
\tag{29}
$$

The on-state durations of the basic vectors for the three-level inverter in the Sextant 1 is

$$
\begin{cases}
T_0 = \left[1 - \sqrt{3} M \sin\left(\pi/3 + \theta\right)\right] T_\text{S} \\[1mm]
T_{10} = \sqrt{3} M T_\text{S} \sin\left(\pi/3 - \theta\right) \qquad \text{(Triangle A)} \\[1mm]
T_{20} = \sqrt{3} M T_\text{S} \sin\theta
\end{cases}
\tag{30}
$$

$$
\begin{cases}
T_{10} = \left(1 - \sqrt{3} M \sin\theta\right) T_\text{S} \\[1mm]
T_{20} = \left[1 - \sqrt{3} M \sin\left(\pi/3 - \theta\right)\right] T_\text{S} \qquad \text{(Triangle B)} \\[1mm]
T_3 = \left[\sqrt{3} M \sin\left(\pi/3 + \theta\right) - 1\right] T_\text{S}
\end{cases}
\tag{31}
$$

$$
\begin{cases}
T_{10} = \left[2 - \sqrt{3} M \sin\left(\pi/3 + \theta\right)\right] T_\text{S} \\[1mm]
T_3 = \sqrt{3} M T_\text{S} \sin\theta \qquad \text{(Triangle C)} \\[1mm]
T_1 = \left[\sqrt{3} M \sin\left(\pi/3 - \theta\right) - 1\right] T_\text{S}
\end{cases}
\tag{32}
$$

$$
\begin{cases}
T_3 = \sqrt{3}MT_{\mathrm{S}}\sin\left(\pi/3 - \theta\right) \\[2mm]
T_2 = \left(\sqrt{3}M\sin\theta - 1\right)T_{\mathrm{S}} & \text{(Triangle D)} \\[2mm]
T_{20} = \left[2 - \sqrt{3}M\sin\left(\pi/3 + \theta\right)\right]T_{\mathrm{S}}
\end{cases}
\tag{33}
$$

Step 4: Compute the duration of each segment based on the modulation strategy and store these durations into a matrix ST. The format is as follows.

$$
\mathrm{ST} = \begin{bmatrix} t_1 & t_2 & t_3 & \cdots & t_Z \end{bmatrix}
\tag{34}
$$

For the commonly used symmetrical 7-segment pulse pattern of the two-level inverter,

$$
\mathrm{ST} = \begin{bmatrix} T_0/4 & T_1/2 & T_2/2 & T_0/2 & T_2/2 & T_1/2 & T_0/4 \end{bmatrix}
\tag{35}
$$

For the symmetrical pulse pattern of the three-level inverter with a control factor k_{c}, in the triangle A

$$
\mathrm{ST} = \begin{bmatrix} k_{\mathrm{c}}T_{20}/2 & T_{10}/2 & T_0/2 & (1 - k_{\mathrm{c}})T_{20} & T_0/2 & T_{10}/2 & k_{\mathrm{c}}T_{20}/2 \end{bmatrix}
\tag{36}
$$

Step 5: Compute the average line voltages using the following equations.

$$
U_r = \frac{1}{T_{\mathrm{S}}}\sum_{i=1}^{Z} \mathrm{S}(r, i) \times \mathrm{ST}(i)\frac{U_{\mathrm{DC}}}{N - 1} \quad (r = 1, 2, 3 \text{ for A, B, C respectively})
\tag{37}
$$

Step 6: Compute ripple currents. The ripple current expressions are piecewise functions, and the kth segment can be expressed using the following universal formulas that are applied to the N-level inverter if N is odd and the $(N-1)$-level inverter if N is even.

$$
\begin{cases}
\Delta i_{\mathrm{AB}}(k, t) = \dfrac{1}{L_\sigma}\sum_{\substack{i=1 \\ i \le k-1}}^{k-1}\left[(\mathrm{S}(1, i) - \mathrm{S}(2, i))\dfrac{U_{\mathrm{DC}}}{N - 1} - U_{\mathrm{AB}}\right]t_i \\[4mm]
\qquad + \dfrac{1}{L_\sigma}\left[(\mathrm{S}(1, k) - \mathrm{S}(2, k))\dfrac{U_{\mathrm{DC}}}{N - 1} - U_{\mathrm{AB}}\right]\left(t - \sum_{\substack{i=1 \\ i \le k-1}}^{k-1}\mathrm{ST}(i)\right) \\[4mm]
\Delta i_{\mathrm{AC}}(k, t) = \dfrac{1}{L_\sigma}\sum_{\substack{i=1 \\ i \le k-1}}^{k-1}\left[(\mathrm{S}(1, i) - \mathrm{S}(3, i))\dfrac{U_{\mathrm{DC}}}{N - 1} - U_{\mathrm{AC}}\right]t_i \\[4mm]
\qquad + \dfrac{1}{L_\sigma}\left[(\mathrm{S}(1, k) - \mathrm{S}(3, k))\dfrac{U_{\mathrm{DC}}}{N - 1} - U_{\mathrm{AC}}\right]\left(t - \sum_{\substack{i=1 \\ i \le k-1}}^{k-1}\mathrm{ST}(i)\right) \\[4mm]
\Delta i_{\mathrm{BC}}(k, t) = \dfrac{1}{L_\sigma}\sum_{\substack{i=1 \\ i \le k-1}}^{k-1}\left[(\mathrm{S}(2, i) - \mathrm{S}(3, i))\dfrac{U_{\mathrm{DC}}}{N - 1} - U_{\mathrm{BC}}\right]t_i \\[4mm]
\qquad + \dfrac{1}{L_\sigma}\left[(\mathrm{S}(2, k) - \mathrm{S}(3, k))\dfrac{U_{\mathrm{DC}}}{N - 1} - U_{\mathrm{BC}}\right]\left(t - \sum_{\substack{i=1 \\ i \le k-1}}^{k-1}\mathrm{ST}(i)\right)
\end{cases}
\tag{38}
$$

Step 7: Analyze ripple current characteristics. For example, the analytical expressions and characteristics of the harmonic distortion factor (HDF) can be gotten from the ripple currents. The HDF is corresponding to the total harmonic distortion (THD) and can be defined using the ripple currents. The micro HDF is defined to evaluate the current THD

in a switching period while the macro HDF is defined to evaluate the current THD in a fundamental period of the implicit modulation wave. The micro HDF is defined as [2]

$$f(M, \theta) = \frac{\frac{1}{T_\mathrm{S}} \int_0^{T_\mathrm{S}} \left(\Delta i_\mathrm{AB}^2 + \Delta i_\mathrm{AC}^2 + \Delta i_\mathrm{BC}^2 \right) \mathrm{d}t}{3 \left(\frac{U_\mathrm{DC}}{2L_\sigma} \right)^2 \frac{T_\mathrm{S}^2}{48}} \tag{39}$$

The macro HDF is defined as [2]

$$F(M) = \frac{1}{2\pi} \int_0^{2\pi} f(M, \theta) \mathrm{d}\theta \tag{40}$$

5. **Analysis and Discussion.**

5.1. **Two-level three-phase inverter.** Because of the pulse symmetry shown in Equations (35) and (36) to some SVPWM schemes, the ripple currents are almost zero at the middle of the switching period and substantially centrosymmetric about the middle. It is sufficient to analyze the ripple currents in the half period.

The random SVPWM strategy can suppress the clustered harmonic amplitude peak value that is the most serious in the deterministic SVPWM strategy [21-23]. Among the most intuitional random schemes, the switching signal waveforms shown in Figure 1(d) and the ripple currents in the random zero-vector distribution SVPWM (RZDSVPWM) scheme are substantially centrosymmetric about the middle. Therefore, the RZDSVPWM scheme can be easily realized in plenty of microcontroller units. For one novel RZDSVP-WM scheme, the matrix ST shown in Equation (34) is given by

$$\mathrm{ST} = \left[\begin{array}{ccccccc} T_{00}/2 & T_1/2 & T_2/2 & T_{07} & T_2/2 & T_1/2 & T_{00}/2 \end{array} \right] \tag{41}$$

where R is a random variable that represents the random zero-vector distribution factor,

$$\begin{cases} T_{00} = RT_{0\min} + \dfrac{1}{2}(T_0 - T_{0\min}) \\ T_{07} = (1 - R)T_{0\min} + \dfrac{1}{2}(T_0 - T_{0\min}) \end{cases} \quad (0 \leq R \leq 1)$$

and

$$T_{0\min} = T_\mathrm{S} \left(1 - \frac{\sqrt{3}}{2}M \right)$$

Using the algorithm stated in Section 4, the micro HDF can be gotten as

$$\begin{aligned} f(M, \theta) = {}& \frac{M^4}{32} \left(\begin{array}{l} -9\cos 4\theta + 72\sqrt{3}R\cos 3\theta - 36\sqrt{3}\cos 3\theta - 18\cos 2\theta \\ -72\sqrt{3}R\cos\theta + 36\sqrt{3}\cos\theta + 9\sqrt{3}\sin 4\theta - 18\sqrt{3}\sin 2\theta \\ +216R\sin\theta - 108\sin\theta + 432R^2 - 432R + 162 \end{array} \right) \\ & + \frac{M^3}{4} \left(\begin{array}{l} -18R\cos 3\theta + 9\cos 3\theta + 18R\cos\theta - 18\cos\theta + \sqrt{3}\sin 3\theta \\ -18\sqrt{3}R\sin\theta + 6\sqrt{3}\sin\theta - 72\sqrt{3}R^2 + 72\sqrt{3}R - 18\sqrt{3} \end{array} \right) \\ & + \left(18R^2 - 18R + 6 \right) M^2 \end{aligned} \tag{42}$$

The macro HDF can be gotten as

$$\begin{aligned} F(M) = {}& \frac{27}{2} \left(R^2 - R - \frac{3\sqrt{3}}{32} + \frac{3}{8} \right) M^4 \\ & + \left(-18\sqrt{3}R^2 + 18\sqrt{3}R - \frac{9\sqrt{3}}{2} - \frac{4\sqrt{3}}{\pi} \right) M^3 \\ & + \left(18R^2 - 18R + 6 \right) M^2 \end{aligned} \tag{43}$$

Let $R = 0.5$, the micro and macro HDF expressions of the commonly used symmetrical 7-segment pulse pattern can be gotten. Therefore, the macro HDF is

$$F(M) = \frac{9}{8}\left(\frac{3}{2} - \frac{9}{8}\cdot\frac{\sqrt{3}}{\pi}\right)M^4 - \frac{4\sqrt{3}}{\pi}M^3 + \frac{3}{2}M^2 \tag{44}$$

Equation (44) is in full accord with the result given and verified by Holmes and Lipo [2]. The correctness and universality of the proposed model and algorithm are consequently confirmed to a great extent.

5.2. **Three-level three-phase inverter.** Using the algorithm stated above, the ripple current characteristic for the symmetrical pulse pattern of a three-level inverter with a control factor k_c will be analyzed. The implicit phase voltage modulation waves $\begin{bmatrix} U_{Ai} & U_{Bi} & U_{Ci} \end{bmatrix}^T$ for $i = 1, 2, 3, 4, 5, 6$ in the six triangles are as follows.

$$\begin{bmatrix} U_{A1} \\ U_{B1} \\ U_{C1} \end{bmatrix} = MU_{DC}\begin{bmatrix} \frac{1}{4}\left(3\cos\theta - \sqrt{3}\sin\theta + 2\sqrt{3}k_c\sin\theta\right) \\ \frac{1}{2}\sqrt{3}k_c\sin\theta \\ \frac{1}{2}\sqrt{3}\left(k_c - 1\right)\sin\theta \end{bmatrix}$$

$$\begin{bmatrix} U_{A2} \\ U_{B2} \\ U_{C2} \end{bmatrix} = MU_{DC}\begin{bmatrix} -\frac{1}{2}\sqrt{3}k_c\sin\left(\theta - \frac{\pi}{3}\right) \\ -\frac{1}{2}\sqrt{3}\left(k_c - 1\right)\sin\left(\theta - \frac{\pi}{3}\right) \\ \frac{1}{2}\sqrt{3}\left(k_c - 1\right)\sin\theta \end{bmatrix}$$

$$\begin{bmatrix} U_{A3} \\ U_{B3} \\ U_{C3} \end{bmatrix} = U_{DC}\begin{bmatrix} \frac{1}{4}\left(2k_c + M\left(1 - k_c\right)\left(3\cos\theta - \sqrt{3}\sin\theta\right)\right) \\ -\frac{1}{2}k_c\left(\sqrt{3}M\sin\left(\frac{\pi}{3} - \theta\right) - 1\right) \\ \frac{1}{4}\left(2k_c - 3Mk_c\cos\theta - \sqrt{3}M\left(2 - k_c\right)\sin\theta\right) \end{bmatrix}$$

$$\begin{bmatrix} U_{A4} \\ U_{B4} \\ U_{C4} \end{bmatrix} = U_{DC}\begin{bmatrix} \frac{1}{2}\left(\sqrt{3}M\sin\left(\frac{\pi}{3} + \theta\right) - 1 - k_c\left(\sqrt{3}M\sin\theta - 1\right)\right) \\ -\frac{1}{2}\left(\sqrt{3}M\sin\theta - 1\right)\left(k_c - 1\right) \\ -\frac{1}{2}\left(\sqrt{3}Mk_c\sin\theta - k_c + 1\right) \end{bmatrix}$$

$$\begin{bmatrix} U_{A5} \\ U_{B5} \\ U_{C5} \end{bmatrix} = U_{DC}\begin{bmatrix} \frac{1}{4}\left(4k_c + M\left(1 - k_c\right)\left(3\cos\theta + \sqrt{3}\sin\theta\right) - 2\right) \\ \frac{1}{2}\left(\sqrt{3}M\sin\theta - 1 - k_c\left(\sqrt{3}M\sin\left(\theta + \frac{\pi}{3}\right) - 2\right)\right) \\ -\frac{1}{4}\left(3Mk_c\left(\cos\theta + \sin\theta\right) - 4k_c + 2\right) \end{bmatrix}$$

$$
\begin{bmatrix} U_{\mathrm{A6}} \\ U_{\mathrm{B6}} \\ U_{\mathrm{C6}} \end{bmatrix} = U_{\mathrm{DC}} \begin{bmatrix} \dfrac{1}{4}\left(4k_{\mathrm{c}} + M\left(1 - k_{\mathrm{c}}\right)\left(3\cos\theta + \sqrt{3}\sin\theta\right) - 2\right) \\[2mm] -\dfrac{1}{4}\left(Mk_{\mathrm{c}}\cos\theta - \sqrt{3}\left(2 - k_{\mathrm{c}}\right)M\sin\theta + 2 - 4k_{\mathrm{c}}\right) \\[2mm] -\dfrac{1}{4}\left(3Mk_{\mathrm{c}}\left(3\cos\theta + \sqrt{3}\sin\theta\right) - 4k_{\mathrm{c}} + 2\right) \end{bmatrix}
$$

The three line voltages expressions are identical in the six triangles, which are shown as follows. This well known fact can be explained through the vector definition and construction Equation (2). The control factor k_{c} has only heavy effect on the zero sequence component and implicit phase voltage modulation waves with respect to the neutral point 0 created by the two identical capacitors C_1 and C_2.

$$
\begin{bmatrix} U_{\mathrm{AB}} \\ U_{\mathrm{AC}} \\ U_{\mathrm{BC}} \end{bmatrix} = \frac{\sqrt{3}}{4} M U_{\mathrm{DC}} \begin{bmatrix} \sqrt{3}\cos\theta - \sin\theta \\ \sqrt{3}\cos\theta + \sin\theta \\ 2\sin\theta \end{bmatrix}^{T}
$$

The ripple current expressions are consistent with Equations (11) to (22). The micro HDF expression $f_i(M,\theta)$ for $i = 1, 2, 3, \ldots, 6$ in each triangle shown in Figure 2(c) can be gotten using Equation (39) and are very complicated. The size of the capacitors C_1 and C_2 has heavy effects on the fluctuation of the neutral voltages. The assumption that capacitors have enough size has important theoretic significance. Because of the symmetry, it is sufficient to analyze the macro HDF in the first 60°-Sextant. The solving process and expressions can be expressed as follows.

(1) $0 \le M \le 1/\sqrt{3}$

$$
\begin{aligned}
F(M) &= \frac{3}{\pi}\left[\int_0^{\pi/6} f_2(M,\theta)\mathrm{d}\theta + \int_{\pi/6}^{\pi/3} f_1(M,\theta)\mathrm{d}\theta\right] \\
&= \frac{27}{16}\left(2 - \frac{\sqrt{3}}{\pi}\right)M^4 - \frac{16\sqrt{3} - 18}{\pi}M^3 + \frac{9}{4}\left(1 - \frac{\sqrt{3}}{\pi}\right)M^2
\end{aligned}
\tag{45}
$$

(2) $1/\sqrt{3} < M \le 2/3$,

$$
\begin{aligned}
F(M) &= \frac{3}{\pi}\left[\int_0^{\theta_1} f_2(M,\theta)\mathrm{d}\theta + \int_{\theta_1}^{\pi/6} f_4(M,\theta)\mathrm{d}\theta + \int_{\pi/6}^{\pi/3-\theta_1} f_3(M,\theta)\mathrm{d}\theta \right. \\
&\quad \left.\left. + \int_{\pi/3-\theta_1}^{\pi/3} f_1(M,\theta)\mathrm{d}\theta \right]\right|_{\theta_1 = \arcsin\left(1/\sqrt{3}M\right) - \pi/3} \\
&= \frac{27}{16}\left(2 + \frac{7\sqrt{3}}{\pi}\right)M^4 - \frac{4}{\pi}\left(4\sqrt{3} + 5\sqrt{3 - \frac{1}{M^2}} + 9\right)M^3 \\
&\quad + \frac{1}{\pi}\left(\frac{99\pi}{4} - 45\arcsin\frac{\sqrt{3}}{3M} + \frac{99\sqrt{3}}{4}\right)M^2 - \frac{1}{\pi}\left(\frac{55}{3}\sqrt{3 - \frac{1}{M^2}} + 18\right)M \\
&\quad + \frac{1}{\pi}\left(5\pi - 10\arcsin\frac{\sqrt{3}}{3M} + \frac{3\sqrt{3}}{2}\right)
\end{aligned}
\tag{46}
$$

(3) $2/3 < M \leq 2/\sqrt{3}$,

$$F(M) = \frac{3}{\pi} \left[\int_0^{\theta_2} f_6(M,\theta)\mathrm{d}\theta + \int_{\theta_2}^{\pi/6} f_4(M,\theta)\mathrm{d}\theta + \int_{\pi/6}^{\pi/3-\theta_2} f_3(M,\theta)\mathrm{d}\theta \right.$$

$$\left. + \int_{\pi/3-\theta_2}^{\pi/3} f_5(M,\theta)\mathrm{d}\theta \right]_{\theta_2=\pi/3-\arcsin\left(1/\sqrt{3}M\right)}$$

$$= \frac{27}{8}\left(1 - \frac{\sqrt{3}}{\pi}\right)M^4 + \frac{1}{16\pi}\left(\begin{array}{c} 128\sqrt{3} + \sqrt{3}\left(1 - \frac{1}{3M^2}\right)\sqrt{1 - \frac{1}{3M^2}} \\ +63\sqrt{1 - \frac{1}{3M^2}} - 576 \end{array} \right)M^3 \qquad (47)$$

$$+ \frac{1}{4\pi}\left(27\pi + 36\arcsin\frac{\sqrt{3}}{3M} - 9\sqrt{3}\right)M^2 + \frac{1}{16\pi}\left(59\sqrt{3 - \frac{1}{M^2}} - 288\right)M$$

$$+ \frac{1}{2\pi}\left(2 + 4\arcsin\frac{\sqrt{3}}{3M} - 3\sqrt{3}\right)$$

Holmes and Lipo [2] presented the resultant closed-form solutions of the macro HDFs of the two-level inverter for several modulation strategies: simple sinusoidal PWM, one-sixth third-harmonic injection PWM, one-quarter third-harmonic injection PWM, space vector PWM, DPWMMIN, DPWMMAX, DPWM0, DPWM2 discontinuous PWM, DPWM1 discontinuous PWM, and DPWM3 discontinuous PWM. The switching frequency of the inverter phase legs for discontinuous modulation is about two-third of that for continuous modulation, so the switching frequency of discontinuous strategies can be increased by 3/2 for the same switching losses. Combined with Equations (45) to (47), the macro HDFs are shown in Figure 5, which shows the prominent harmonic distortion difference between the three-level inverter and the commonly used two-level inverter. It can be found that the number of the levels, the zero-vector distribution factor and the modulation index have
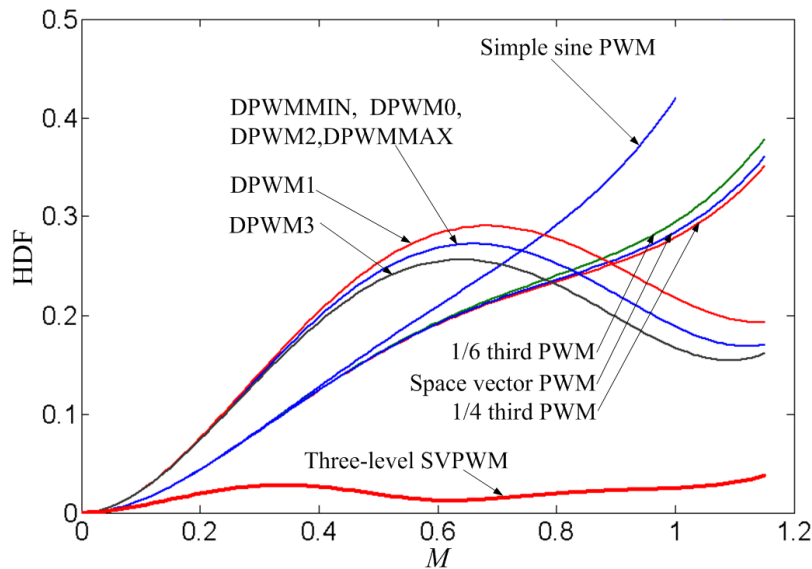

FIGURE 5. Harmonic distortion factors (HDF) for three-level inverter space vector PWM and different modulation strategies of two-level space vector PWM with discontinuous strategy switching frequencies increased by 3/2

heavy effect on the ripple current, usually evaluated using the HDF. The HDF of the three-level inverter does not depend on the zero-vector distribution factor (called control factor) in Equation (36), while the HDF of the two-level inverter highly depends on the zero-vector distribution factor. The essential difference of the SVPWM of the two-level inverter shown in Figure 5 lies in the zero-vector distribution factor. The distribution factor is either 1 or 0 for DPWM0, DPWM1, DPWM2, DPWM3, DPWMMIN and DPWMAX, while the distribution factor is a constant value 0.5 for the space vector PWM in Figure 5. The HDF reaches the maximum value if the modulation index is about 0.65 for the 6 discontinuous PWM strategies, while the HDF presents a very small value in the whole linear modulation range for the three-level inverter.

6. **Conclusions.** The ripple current and harmonic distortion depends very heavily on the topology of the inverter and the PWM strategy. There are many strategies and more new strategies are expected in the future. The quantitative and qualitative analysis of the harmonic distortion and ripple current plays an important role in assessing the performance. The derivation process is tedious and the expression is very complicated, so the universal formulas for the ripple current formulations for space vector PWM (SVPWM) were given. And then a programming algorithm for ripple current analysis for the multilevel inverter was proposed. Additionally, the ripple current and harmonic distortion for a two-level inverter and a three-level one were discussed using the algorithm, which verifies its convenience and practicability. The universal ripple formulas and algorithm are fully applicable to all kinds of space vector PWM strategies. Therefore, it provides a powerful tool for accurately comparing the harmonic distortion performance among different PWM strategies and different level inverters, and even applicable to exploiting new PWM strategy. In the future, the proposed universal formulations and computation algorithm may be utilized to develop new SVPWM strategies. For example, if the HDF is set as the objective function, the duration of each segment in Equation (34) can be determined using the optimization method, and a current harmonic optimal strategy can be developed.

REFERENCES

[1] X. Mao, A. K. Jain and R. Ayyanar, Hybrid interleaved space vector PWM for ripple reduction in modular converters, *IEEE Trans. Power Electronics*, vol.26, no.7, pp.1954-1967, 2011.

[2] D. G. Holmes and T. A. Lipo, *Pulse Width Modulation for Power Converters: Principles and Practice*, IEEE Press, USA, 2003.

[3] B. K. Bose, *Modern Power Electronics and AC Drives*, Prentice Hall, UK, 2001.

[4] G. Chen, *PWM Inverter Technology and Application*, China Electric Power Press, China, 2007.

[5] B. A. Rahiman, K. Saikrishna, A. H. Khalifa and D. Apparao, Space-vector-based synchronized three-level discontinuous PWM for medium-voltage high-power VSI, *IEEE Trans. Industrial Electronics*, vol.61, no.8, pp.3891-3901, 2014.

[6] P. N. Reddy, J. Amarnath and P. L. Reddy, Hybrid random PWM algorithm for direct torque controlled induction motor drive for reduced harmonic distortion, *Annual IEEE India Conference: Engineering Sustainable Solutions (INDICON-2011)*, Hyderabad, India, 2011.

[7] S. Kaboli, J. Mahdavi and A. Agah, Application of random PWM technique for reducing the conducted electromagnetic emissions in active filters, *IEEE Trans. Industrial Electronics*, vol.54, no.4, pp.2333-2343, 2007.

[8] S. H. Na, Y. G. Jung, Y. C. Lim and S. H. Yang, Reduction of audible switching noise in induction motor drives using random position space vector PWM, *IEE Proceedings – Electric Power Applications*, vol.149, no.3, pp.195-200, 2002.

[9] S. Albatran, Y. Fu and A. Albanna, Comprehensive mathematical description and harmonic analysis of hybrid two-dimensional-three-dimensional space vector modulation, *IEEE Trans. Industrial Electronics*, vol.61, no.7, pp.3327-3336, 2014.

[10] M. Zigliotto and A. M. Trzynadlowski, Effective random space vector modulation for EMI reduction in low-cost PWM inverters, *Proc. of the 7th International Conference on Power Electronics and Variable Speed Drives*, Stevenage, United Kingdom, pp.163-167, 1998.

[11] N. Boudjerda, A. Boudouda, M. Melit, B. Nekhoul, K. E. K. Drissi and K. Kerroum, Optimized dual randomized PWM technique for reducing conducted EMI in DC-AC converters, *The 10th International Symposium on Electromagnetic Compatibility (EMC Europe 2011)*, York, United Kingdom, 2011.

[12] D. Jiang and F. Wang, Variable switching frequency PWM for three-phase converters based on current ripple prediction, *IEEE Trans. Power Electronics*, vol.28, no.11, pp.4951-4961, 2013.

[13] G. Chen, Z. Wu and Y. Zhu, Harmonic analysis of random pulse position space vector PWM, *Journal of Tongji University*, vol.40, no.7, pp.1111-1117, 2012.

[14] Z. Wu, G. Chen, Y. Zhu and G. Tian, Harmonic analysis of random zero-vector distribution space vector pulse-width modulation, *Journal of Tongji University*, vol.39, no.9, pp.901-907, 2011.

[15] G. Chen, M. Zhang and J. Zhao, Harmonic distortion factor of a hybrid space vector PWM based on random zero-vector distribution and random pulse position, *Advances in Information Sciences and Service Sciences*, vol.4, no.16, pp.242-250, 2012.

[16] D. Dujic, M. Jones, L. Emil, J. Prieto and F. Barrero, Switching ripple characteristics of space vector PWM schemes for five-phase two-level voltage source inverters – Part 1: Flux harmonic distortion factors, *IEEE Trans. Industrial Electronics*, vol.58, no.7, pp.2789-2798, 2011.

[17] J. Holtz, M. Holtgen and J. O. Krah, A space vector modulator for the high-switching frequency control of three-level SiC inverters, *IEEE Trans. Power Electronics*, vol.29, no.5, pp.2618-2626, 2014.

[18] N. Celanovic and D. Boroyevich, A comprehensive study of neutral-point voltage balancing problem in three-level neutral-point-clamped voltage source PWM inverters, *IEEE Trans. Power Electronics*, vol.15, no.2, pp.242-249, 2000.

[19] L. Dai, X. Chen, Z. Yu and Y. Fu, Three-level inverter and its simulation, *Journal of University of Sciences and Technology Liaoning*, vol.34, no.1, pp.360-367, 2011.

[20] Y. Chen, Y. Li and L. Zhao, A novel SVPWM algorithm considering neutral-point potential balancing for three-level NPC inverter, *Electronics*, vol.20, no.2, pp.69-75, 2016.

[21] G. Chen and J. Kang, Harmonic analysis of a random zero vector distribution space vector pulse width modulation, *International Journal of Signal Processing, Image Processing and Pattern Recognition*, vol.9, no.6, pp.227-240, 2016.

[22] T. S. Sivarani, J. S. Joseph and K. C. Agees, Intensive random carrier pulse width modulation for induction motor drives based on hopping between discrete carrier frequencies, *IET Power Electronics*, vol.9, no.3, pp.417-426, 2016.

[23] A. Peyghambari, A. Dastfan and A. Ahmadyfard, Strategy for switching period selection in random pulse width modulation to shape the noise spectrum, *IET Power Electronics*, vol.8, no.4, pp.517-523, 2015.